CANCER

Targeted antibody and cytokine cancer immunotherapies through collagen affinity

Jun Ishihara[1]*, Ako Ishihara[1]*, Koichi Sasaki[1†], Steve Seung-Young Lee[2], John-Michael Williford[1], Mariko Yasui[3], Hiroyuki Abe[3], Lambert Potin[1,4], Peyman Hosseinchi[1], Kazuto Fukunaga[1‡], Michal M. Raczy[1], Laura T. Gray[1], Aslan Mansurov[1], Kiyomitsu Katsumata[1§], Masashi Fukayama[3], Stephen J. Kron[2], Melody A. Swartz[1,5], Jeffrey A. Hubbell[1||]

Cancer immunotherapy with immune checkpoint inhibitors (CPIs) and interleukin-2 (IL-2) has demonstrated clinical efficacy but is frequently accompanied with severe adverse events caused by excessive and systemic immune system activation. Here, we addressed this need by targeting both the CPI antibodies anti–cytotoxic T lymphocyte antigen 4 antibody (αCTLA4) + anti–programmed death ligand 1 antibody (αPD-L1) and the cytokine IL-2 to tumors via conjugation (for the antibodies) or recombinant fusion (for the cytokine) to a collagen-binding domain (CBD) derived from the blood protein von Willebrand factor (VWF) A3 domain, harnessing the exposure of tumor stroma collagen to blood components due to the leakiness of the tumor vasculature. We show that intravenously administered CBD protein accumulated mainly in tumors. CBD conjugation or fusion decreases the systemic toxicity of both αCTLA4 + αPD-L1 combination therapy and IL-2, for example, eliminating hepatotoxicity with the CPI molecules and ameliorating pulmonary edema with IL-2. Both CBD-CPI and CBD–IL-2 suppressed tumor growth compared to their unmodified forms in multiple murine cancer models, and both CBD-CPI and CBD–IL-2 increased tumor-infiltrating $CD8^+$ T cells. In an orthotopic breast cancer model, combination treatment with CPI and IL-2 eradicated tumors in 9 of 13 animals with the CBD-modified drugs, whereas it did so in only 1 of 13 animals with the unmodified drugs. Thus, the A3 domain of VWF can be used to improve safety and efficacy of systemically administered tumor drugs with high translational promise.

INTRODUCTION

Immune checkpoint inhibitors (CPIs) have demonstrated clinical efficacy in cancer immunotherapy (*1*, *2*). Immune checkpoints are inhibitory pathways used by the immune system to protect cells from excessive immune responses (*3*). Cytotoxic T lymphocyte antigen 4 (CTLA4; CD152) is expressed on regulatory T cells (T_{regs}) and activated T cells (*4*, *5*). In the clinic, anti-CTLA4 antibody (αCTLA4) treatment prolonged survival of patients with melanoma (*5*). Some tumor cells express programmed death ligand 1 (PD-L1; CD274). Association of PD-L1 with its receptor programmed death 1 (PD-1; CD279) results in inactivation of T cells. Anti–PD-L1 (αPD-L1) blocking antibodies have shown efficacy against several types of cancer (*6*, *7*). Moreover, combination therapy using anti–PD-1 (αPD-1; nivolumab) and αCTLA4 (ipilimumab) shows prolongation of survival (*8*) and has been approved by the U.S. Food and Drug Administration (FDA) for treatment of advanced melanoma and renal cell carcinoma. However, CPI treatment also shows severe side effects, including immune-related adverse events (*8*–*10*). In combination therapy, 96% of patients experienced adverse events, and 36% of patients discontinued therapy due to adverse events (*8*).

Interleukin-2 (IL-2; aldesleukin) is a cytokine that induces proliferation and activation of T cells and natural killer cells (NK cells) (*11*). Administration of IL-2 has exhibited antitumor effects in the clinic (*12*), and aldesleukin has been approved by the FDA for treatment of metastatic melanoma and renal cell carcinoma. In clinical studies, 19% of patients responded to aldesleukin with prolonged survival, but almost all patients experienced treatment-related adverse events, including 1.1% of treatment-related death (*13*). Aldesleukin has a narrow therapeutic window due to induction of severe adverse events such as pulmonary edema (*14*).

Because such immunotherapeutics serve to activate immune responses, their side effects are caused by immune activation (*10*, *15*) and typically result from off tumor-target drug action. In a way, patients experiencing adverse events have "responded" to the therapy, because their immune systems have been activated by treatment, but converting these cases into positive clinical outcomes remains an important challenge in the field. One strategy to address this problem is through drug-targeting approaches, which seek to deliver drugs only where they are needed, thereby focusing their actions on the disease site. We have previously reported that conjugation of a promiscuous extracellular matrix (ECM)–binding peptide derived from placenta growth factor–2 (specifically, $PlGF\text{-}2_{123-144}$) to CPI antibodies enhanced retention of these antibodies at the peritumoral injection site (*16*). $PlGF\text{-}2_{123-144}$ conjugation enhances antitumor efficacy and safety of αCTLA4 + αPD-L1 combination therapy compared to their unmodified forms when injected locally. This approach requires local intra/peritumoral injection; although local injection of $PlGF\text{-}2_{123-144}$–CPI improved CPI therapy, administration of the drug systemically and having it target to the tumor sites from the blood would improve translational utility and increase the range of applicable cancer types and patients.

[1]Institute for Molecular Engineering, University of Chicago, Chicago, IL 60637, USA. [2]Department of Molecular Genetics and Cell Biology, University of Chicago, Chicago, IL 60637, USA. [3]Department of Pathology, University of Tokyo, 113-8655 Tokyo, Japan. [4]Institute of Bioengineering, Ecole Polytechnique Fédérale de Lausanne, CH-1015 Lausanne, Switzerland. [5]Ben May Department for Cancer Research, University of Chicago, Chicago, IL 60637, USA.
*These authors contributed equally to this work.
†Present address: Department of Applied Chemistry, Faculty of Engineering, Kyushu University, 819-0395 Fukuoka, Japan.
‡Present address: FUJIFILM Corporation, 258-8577 Kanagawa, Japan.
§K.K. is on leave from Astellas Pharma Inc.
||Corresponding author. Email: jhubbell@uchicago.edu

Collagen is the most abundant protein in the mammalian body and exists in almost all tissues (*17*). Collagen, an ECM protein, is richly present in the subendothelial space of the blood vessel and the tumor stroma. Because of its insolubility under physiological conditions, collagen barely exists within the blood (*18*, *19*). The vasculature of tumors is hyperpermeable compared to the normal blood vessel, due to an abnormal structure (*20*). Thus, with this leakiness, collagen in the tumor can be exposed to molecules carried in the bloodstream preferentially to other tissues (*21*–*23*). Moreover, many tumor tissues contain increased amounts of collagen compared to normal tissues (*24*, *25*).

von Willebrand factor (VWF), a hemostasis factor, binds to both type I and III collagen (*26*). When a blood vessel is injured, collagen beneath the endothelial cells is exposed to proteins in the blood, and VWF binding to collagen initiates the thrombosis cascade (*26*). The VWF A domain has the highest affinity for collagen among reported nonbacterial origin proteins/peptides (*27*). Particularly within the A domain, the A3 domain of VWF has been reported as a collagen-binding domain (CBD; using this abbreviation to refer specifically to the VWF A3 CBD) (*28*). Here, we hypothesized that CBD conjugation to CPI antibodies and fusion to cytokines such as IL-2 can target these immunotherapeutic molecules to tumors due to the leaky vasculature within the tumor tissue, leading to improved safety and antitumor efficacy by efficient immune system activation within the tumor microenvironment.

RESULTS

CBD-conjugated CPI and CBD-fused IL-2 bind to collagens

We first examined the capacities of CBD-conjugated CPI (CBD-CPI) and CBD-fused IL-2 recombinant protein (CBD–IL-2) to bind collagen in vitro. CPI antibodies were chemically conjugated to human VWF A3 domain recombinant protein (Fig. 1A). Human CBD-fused murine IL-2 was expressed recombinantly. Mass spectrometry (MS) analysis and SDS–polyacrylamide gel electrophoresis (SDS-PAGE) revealed that up to three CBD protein domains were bound to one immunoglobulin G (IgG) and exactly one CBD protein was fused to one IL-2 (fig. S1). Strong binding affinities of CBD-αCTLA4, CBD–αPD-L1, and CBD–IL-2 against type I and III collagen were observed (Fig. 1B and fig. S2). CBD-αCTLA4 and CBD–αPD-L1 recognized their target antigens, and CBD–IL-2 bound to IL-2Rα with similar dissociation constant (K_D) values compared to their unmodified forms (Fig. 1B and fig. S2). CBD–mouse IL-2 and mouse IL-2 induced similar proliferation of the IL-2–dependent CTLL-2 cell line (fig. S3A). In addition, both CBD–human IL-2 and human IL-2 bound to cultured human $CD8^+$ T cells in peripheral blood mononuclear cells (PBMCs; fig. S3B). These data thus show that CBD-CPI

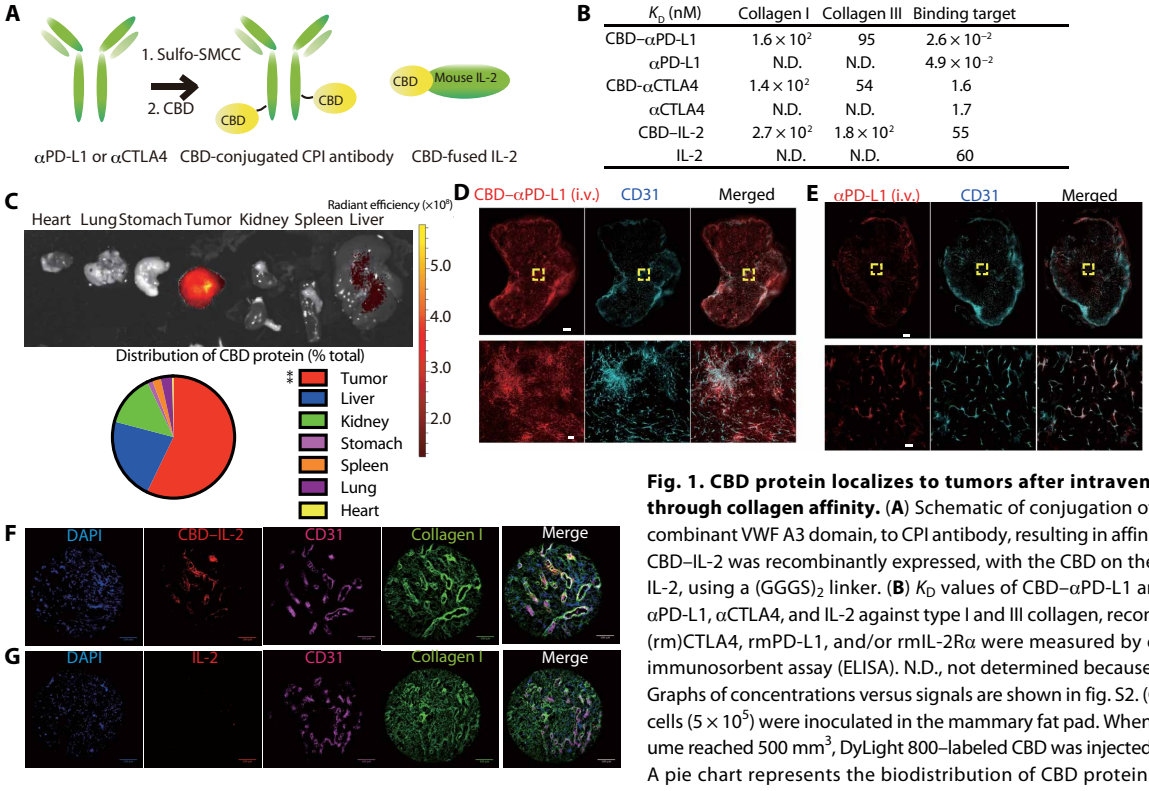

K_D (nM)	Collagen I	Collagen III	Binding target
CBD–αPD-L1	1.6×10^2	95	2.6×10^{-2}
αPD-L1	N.D.	N.D.	4.9×10^{-2}
CBD-αCTLA4	1.4×10^2	54	1.6
αCTLA4	N.D.	N.D.	1.7
CBD–IL-2	2.7×10^2	1.8×10^2	55
IL-2	N.D.	N.D.	60

Fig. 1. CBD protein localizes to tumors after intravenous injection through collagen affinity. (**A**) Schematic of conjugation of a CBD, the recombinant VWF A3 domain, to CPI antibody, resulting in affinity for collagen. CBD–IL-2 was recombinantly expressed, with the CBD on the N terminus of IL-2, using a $(GGGS)_2$ linker. (**B**) K_D values of CBD–αPD-L1 and unmodified αPD-L1, αCTLA4, and IL-2 against type I and III collagen, recombinant mouse (rm)CTLA4, rmPD-L1, and/or rmIL-2Rα were measured by enzyme-linked immunosorbent assay (ELISA). N.D., not determined because of low signals. Graphs of concentrations versus signals are shown in fig. S2. (**C**) MMTV-PyMT cells (5×10^5) were inoculated in the mammary fat pad. When the tumor volume reached 500 mm^3, DyLight 800–labeled CBD was injected intravenously. A pie chart represents the biodistribution of CBD protein 48 hours after injection as determined by fluorescence analysis of each organ ($n = 4$). (**D**) Intratumoral imaging was performed on MMTV-PyMT tumors when they reached 200 mm^3 by injecting DyLight 594–labeled CBD–αPD-L1 or (**E**) DyLight 594–labeled αPD-L1 intravenously (i.v.) 30 min after injection. The tumor was then harvested, and fluorescence was analyzed by microscopy. Top: Images of whole tumors. Scale bar, 500 μm. Bottom: Images of enlarged yellow squares within top panels. Scale bar, 50 μm. Representative images of two tumors each. (**F** and **G**) Binding of (F) CBD–IL-2 or (G) unmodified IL-2 to human melanoma cryosections was imaged by fluorescence microscopy. DAPI, 4′,6-diamidino-2-phenylindole. Scale bars, 100 μm. Two experimental replicates. Statistical analyses were performed using one-way analysis of variance (ANOVA) with Tukey's test. $^{**}P < 0.01$.

and CBD–IL-2 bind to collagens without impairment of their binding capacities to their targets.

CBD protein localizes in the tumor after intravenous injection

We performed an in vivo biodistribution analysis to determine whether CBD localizes in the tumor microenvironment after intravenous injection through binding to endogenous collagen in orthotopic mouse mammary tumor virus–polyomavirus middle T antigen (MMTV-PyMT) breast tumor–bearing mice. Fluorescence detection revealed that the CBD protein preferentially localized in the tumor, with lesser localization in the kidney and liver, where the endothelium is fenestrated (Fig. 1C). We then analyzed the localization of the injected CBD–αPD-L1 within the tumor (Fig. 1, D and E). We observed that intravenously injected CBD–αPD-L1, but not unmodified αPD-L1, localized within the stroma, demonstrating greater tumor retention of the CBD–αPD-L1 compared to αPD-L1 (Fig. 1, D and E, and fig. S4). These data demonstrate tumor targeting of CBD after intravenous injection. CBD–IL-2, but not unmodified IL-2, bound around the blood vessels, where type I collagen is enriched, within human melanoma sections (Fig. 1, F and G).

CBD conjugation to CPI and CBD fusion to IL-2 reduce their side effects

Because the CBD targeted the tumor, we hypothesized that conjugation or fusion of the CBD to immunotherapeutic drugs would reduce toxicity. The concentrations of both CBD-αCTLA4 and CBD–αPD-L1 in blood serum were lower compared to their unmodified forms (fig. S5, A and B). This is presumably due to sequestration of CBD-CPI within the tumor and thus competition of the tumor against the nondiseased tissues. Administration of unmodified CPI (αCTLA4 and αPD-L1 in combination) to B16F10 tumor–bearing mice increased tumor necrosis factor–α (TNFα) concentrations in serum (indicative of excess activation of the immune system) and induced marked morphological changes and leukocyte infiltration in the lung and the liver, whereas CBD-CPI did not (Fig. 2, A to C, and fig. S6A). No statistically significant elevations of leukocyte infiltration were observed in the kidney in either case (fig. S6B). CPI treatment induced $CD8^+$ T cell but not $CD4^+$ T cell, B cell, or NK cell infiltration into the liver (fig. S7). Unmodified CPI, but not CBD-CPI treatment, increased both alanine aminotransferase (ALT) and aspartate aminotransferase (AST) activity, clinically used liver damage markers, in serum (Fig. 2, D and E). An increase of water content in the liver was induced by CPI but not CBD-CPI therapy, suggesting that CBD-CPI therapy maintains the liver structure (Fig. 2F). Injected CBD–IL-2 demonstrated shorter plasma half-life compared to that of unmodified IL-2 in tumor-bearing mice (fig. S5C). In non–tumor-bearing mice, CBD–IL-2 and IL-2 showed similar plasma half-life. Faster clearance of CBD–IL-2 in tumor-bearing mice is presumably due to competition from the tumor for binding. Unmodified IL-2 administration induced splenomegaly and pulmonary edema due to increased vascular permeability (*29*), whereas CBD–IL-2 did not (Fig. 2, G and H). Together, these results indicate that CBD conjugation decreases systemic toxicity of both CPI and IL-2 immunotherapy.

CBD conjugation to CPI and CBD fusion to IL-2 improve efficacy in multiple cancer models

We then examined the antitumor efficacy of CBD-αCTLA4 + CBD–αPD-L1 combination therapy. In B16F10 melanoma, unmodified CPI treatment exhibited small antitumor effects under this regimen (Fig. 3A). In contrast, CBD-CPI at the same dose as unmodified CPI displayed a further therapeutic effect, slowing tumor growth

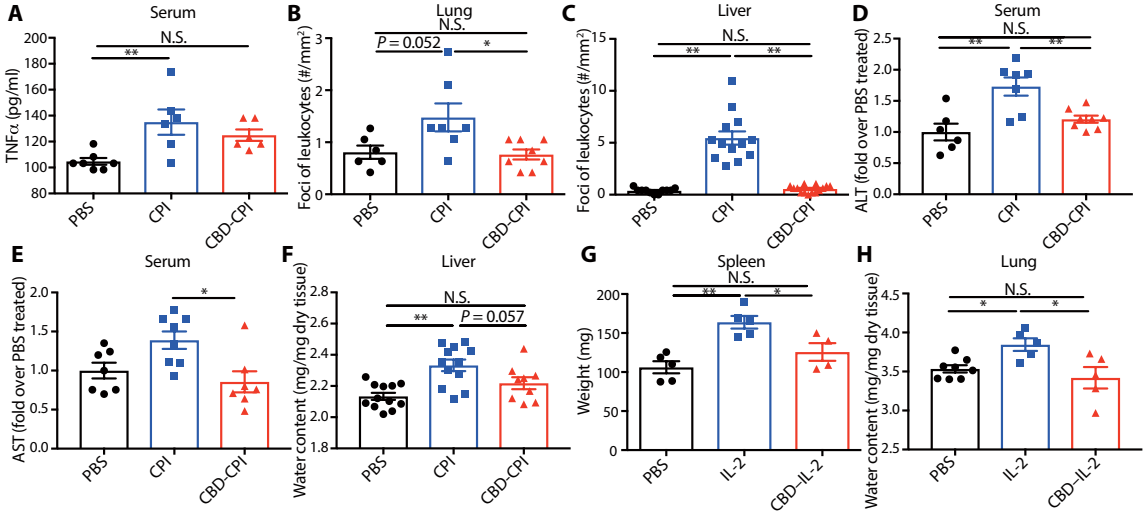

Fig. 2. CBD fusion reduces treatment-related toxicity of immunotherapeutic drugs. Adverse events were studied in mice bearing B16F10 melanomas. B16F10 cells (5×10^5) were inoculated on day 0. (**A** to **F**) αCTLA4 and αPD-L1 were injected intravenously on days 4 and 7. (A) On day 8, serum concentrations of TNFα in blood plasma were measured (means ± SEM). (B and C) On day 10, the numbers of leukocytic infiltration spots in histologic (B) lung and (C) liver sections were counted and divided by area (means ± SEM). (D and E) On day 10, blood serum (D) ALT and (E) AST activities were measured (means ± SEM). (F) On day 10, the liver was harvested and weighed. Water content in the liver was determined by weighing before and after lyophilization and was normalized to dry tissue weight (means ± SEM). (**G** and **H**) B16F10 cells (5×10^5) were inoculated on day 0. CBD–IL-2 or unmodified IL-2 was injected intravenously on days 7 to 9. On day 10, the (G) spleen and (H) lung were harvested and weighed. Water content in the lung was determined as described above (means ± SEM). Statistical analyses were performed using ANOVA with Tukey's test. Kruskal-Wallis test followed by Dunn's multiple comparison was used in (C) due to nonparametric data. Two experimental replicates. $^*P < 0.05$, $^{**}P < 0.01$. N.S., not significant; PBS, phosphate-buffered saline.

(Fig. 3A) at both 25 and 100 μg of single doses of each antibody. Administration of CPI + CBD protein without conjugation abolished the antitumor effect, indicating that the conjugation of CBD to CPI is indispensable for this action and that free CBD has no intrinsic antitumor activity (fig. S8). We also compared the efficacy of CBD-CPI administered systemically to our earlier published approach on local peritumoral administration of ECM-binding PlGF-$2_{123–144}$–αCTLA4 and PlGF-$2_{123–144}$–αPD-L1 (*16*); we observed that systemic

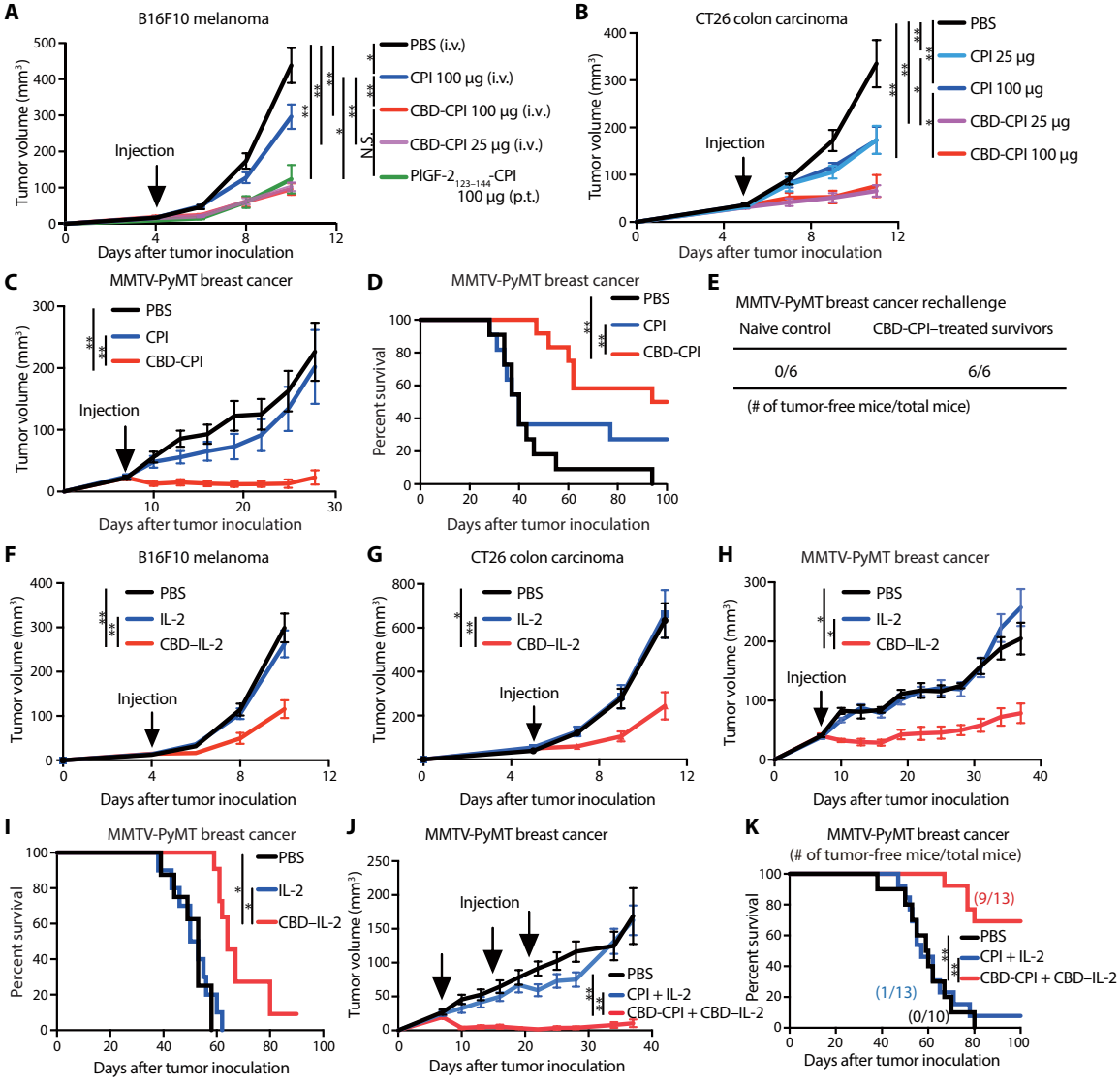

Fig. 3. Both CBD-CPI and CBD–IL-2 treatments reduce tumor growth in three murine tumor models. We used three tumor models to study the efficacy of targeted immunotherapy, namely, the B16F10 melanoma model, the CT26 colon carcinoma model, and the MMTV-PyMT breast cancer model. (**A**) A total of 5×10^5 B16F10 cells were inoculated on back skin, (**B**) 5×10^5 CT26 cells were inoculated on back skin, and (**C** and **D**) 5×10^5 MMTV-PyMT cells were inoculated on the right mammary fat pad on day 0. (A to D) CBD-αCTLA4 + CBD–αPD-L1 (CBD-CPI), αCTLA4 + αPD-L1 (CPI), or PBS was administered on (A) day 4, (B) day 5, and (C and D) day 7. (A) CBD-CPI and unmodified CPI were injected intravenously, and PlGF-$2_{123–144}$–CPI was injected peritumorally (p.t.). Antibody doses per administration are indicated on the figure. Graphs depict (A to C) tumor volume until the first mouse died and (D) survival rate. (**E**) Thirty days after the first tumor inoculation in the right mammary gland fat pad, 5×10^5 MMTV-PyMT cells were again inoculated into the left mammary gland fat pad in CBD-CPI–treated tumor-free survivors or in naïve mice. Numbers indicate how many mice remained tumor free among total mice after 40 days of tumor rechallenge. (**F**) A total of 5×10^5 B16F10 cells were inoculated on the back skin, (**G**) 5×10^5 CT26 cells were inoculated on the back skin, and (**H** to **K**) 5×10^5 MMTV-PyMT cells were inoculated on the right mammary fat pad on day 0. (F to I) IL-2 or equimolar CBD–IL-2 was injected intravenously on (F) day 4, (G) day 5, and (H and I) day 7. Graphs depict (F to H) tumor volume until the first mouse died and (I) survival rate. (J and K) After 7, 14, and 21 days from tumor inoculation, CBD-αCTLA4 + CBD–αPD-L1 (CBD-CPI) + CBD–IL-2, αCTLA4 + αPD-L1 (CPI) + IL-2, or PBS were injected intravenously. Graphs depict (J) tumor volume until the first mouse died and (K) survival rate. Numbers indicate how many mice remained tumor free among total mice 100 days after tumor inoculation. (A) PBS, $n = 9$; CPI (100 μg) and CBD-CPI (25 μg), $n = 8$; CBD-CPI (100 μg) and PlGF-$2_{123–144}$–CPI (100 μg), $n = 7$. (B) PBS and CPI (25 μg), $n = 11$; CPI (100 μg) and CBD-CPI (25 μg), $n = 10$; CBD-CPI (100 μg), $n = 9$. (C and D) CBD-CPI, $n = 12$; other groups, $n = 11$. (E to G) $n = 6$. (H and I) PBS, $n = 10$; other groups, $n = 11$. (J and K) PBS, $n = 10$; other groups, $n = 13$. Tumor volumes are presented as means ± SEM. Two experimental replicates. Statistical analyses were performed using ANOVA with Tukey's test for tumor size and log-rank (Mantel-Cox) test for survival curves. $^*P < 0.05$, $^{**}P < 0.01$.

targeting of the CBD-CPI molecules achieved similar efficacy as the local administration of the PlGF-$2_{123–144}$–CPI molecules at equal doses (Fig. 3A). In the case of a CT26 colon carcinoma, a single dose of unmodified CPI slowed tumor progression; equidosed CBD-CPI treatment further suppressed tumor growth (Fig. 3B). CBD-CPI also showed higher antitumor efficacy against MMTV-PyMT breast tumors and extended survival of mice compared to unmodified CPI (Fig. 3, C and D). A single dose of CBD-CPI led to complete remission in 6 of 12 mice, and no mice rechallenged with MMTV-PyMT cells developed palpable tumors, whereas all naïve mice grew detectable tumors, demonstrating that CBD-CPI induced immunologic memory (Fig. 3E). CBD-CPI did not show a response against EMT6 breast cancer, which is reportedly an immune-excluded tumor, in which there is an antitumor immune response but the immune cells are not able to penetrate into the tumor microenvironment (fig. S9A) (*30*).

Next, we examined the antitumor efficacy of CBD–IL-2. Six micrograms of IL-2 or equimolar CBD–IL-2 was injected intravenously in B16F10 tumor–bearing mice. At this dose, unmodified IL-2 treatment did not show a clear antitumor effect, consistent with a previous report (*31*), whereas CBD–IL-2 treatment induced smaller tumor sizes (Fig. 3F). Similarly, CBD–IL-2, but not unmodified IL-2, showed antitumor effects against CT26 and MMTV-PyMT tumors (Fig. 3, G to I). CBD–IL-2 slightly delayed EMT6 tumor growth (fig. S9B). This set of data indicates that CBD–IL-2 therapy has superior antitumor effects compared to its unmodified form. Combination therapy of CBD-CPI + CBD–IL-2 administration further suppressed MMTV-PyMT tumor growth and extended survival (Fig. 3, J and K). Combined CBD-CPI + CBD–IL-2 administration induced complete remission in 9 of 13 mice, whereas unmodified control CPI + IL-2 treatment did so in 1 of 13 mice.

CBD-CPI and CBD–IL-2 enhance antitumor immunity compared to their unmodified forms

To determine the mechanism behind the therapeutic action of CBD-CPI and CBD–IL-2 treatments, we characterized T cell responses in B16F10 tumor–bearing mice. CBD-CPI increased the frequency of $CD8^+$ T cells of total $CD45^+$ cells within the tumor compared to unmodified CPI and PBS injection (Fig. 4A), whereas the frequency of $CD4^+$ T cells was maintained in all groups (Fig. 4B). CBD-CPI treatment, but not CPI treatment, decreased the percentage of $CD25^+Foxp3^+$ T_{regs} within the $CD4^+$ T cell population (Fig. 4C). As a consequence, CBD-CPI treatment enhanced effector ($CD62L^-CD44^+$) $CD8^+$ T cell–to-T_{reg} ratios within the tumor, a predictor of therapeutic efficacy (*32*), compared to equidosed unmodified CPI and PBS treatments (Fig. 4D). To test whether tumor-infiltrating $CD8^+$ T cells produced higher concentrations of effector cytokines, $CD8^+$ T cells were stimulated ex vivo using αCD3 and αCD28. CBD-CPI treatment increased the percentage of IL-2^+, TNFα^+, and interferon-γ–positive (IFNγ^+) cells in $CD8^+$ tumor-infiltrating T cells compared to the PBS treatment group, whereas unmodified CPI treatment did not (Fig. 4, E to G). CBD-CPI reduced the frequency of macrophages and granulocytic myeloid-derived suppressor cells (MDSCs), which are immunosuppressive cells, as well as dendritic cells within the tumor (fig. S10).

As to B16F10 melanoma tumor immune responses to IL-2 treatment, CBD–IL-2 treatment enhanced the number and frequency of tumor-infiltrating $CD8^+$ T cells (Fig. 4, H and I). CBD–IL-2 therapy did not increase the expression of the exhaustion marker PD-1 in these $CD8^+$ T cells (fig. S11A). Neither IL-2 nor CBD–IL-2 increased the frequency and number of $CD4^+$ T cells or NK cells within the tumor (Fig. 4, J and K, and fig. S11, B and C). CBD–IL-2 increased the frequency of T_{regs} within $CD4^+$ T cells, to the same extent as IL-2 (fig. S11, D and E). CBD–IL-2 did not significantly increase the number of T_{regs}. CBD–IL-2 did not increase other immune suppressive cells such as MDSCs or macrophages within the tumor (fig. S11, F to H). The frequency of $CD8^+$ T cells within the spleen was unchanged after CBD–IL-2 therapy (fig. S11I), suggesting tumor-specific $CD8^+$ T cell expansion. CBD–IL-2 did not affect the frequencies of PD-1^+CD8^+ T cells within total $CD8^+$ T cells or the frequencies of $CD4^+$ T cells, granulocytic MDSCs, or macrophages in the spleen (fig. S11, J to M). CBD–IL-2 slightly increased the frequency of NK cells and slightly decreased the frequency of myelomonocytic MDSCs in the spleen (fig. S11, N and O).

In the breast cancer models, CBD–IL-2, but not IL-2, increased the numbers of $CD8^+$ T cells and NK cells within the MMTV–PyMT tumor but did not change the numbers of $CD4^+$ T cells, the frequencies of PD-1^+CD8^+ T cells, or T_{regs} (fig. S12, A to E). In contrast, neither CBD–IL-2 nor IL-2 treatment affected the number of $CD8^+$, PD-1^+CD8^+, $CD4^+$ T cells, T_{regs}, or NK cells within the immune-excluded EMT6 tumor (fig. S12, F and J). Collectively, CBD-CPI and CBD–IL-2 treatment effectively activated tumor-infiltrating T cells, corresponding to the therapeutic effects observed in Fig. 3.

DISCUSSION

Strategies of targeted tumor therapy can be classified as active targeting or passive targeting (*33*). Previously, as active targeting strategies, antibodies against proteins that are specifically expressed on tumor cells or in the tumor microenvironment have been developed, including those targeting fibronectin extra domain A, fibroblast activation protein α, carcinoembryonic antigen, and mucin (*34*–*37*). Drug conjugates or fusions to these antibodies have shown benefits of tumor targeting. CBD-based tumor targeting is also an active targeting approach, in terms of tumor collagen targeting based on molecular affinity, but it targets a protein that is abundant both throughout the body and in the tumor. CBD-based tumor targeting exploits the pathological structure of tumor vessels, where the vasculature is more permeable than in healthy tissues (*38*, *39*). Thus, the CBD-modified drugs are tumor microenvironment specific, yet not by targeting a molecule that is specifically located in the tumor, but rather exploiting tumor-specific accessibility. The CBD may be usable without previous investigation of tumor antigens, because collagen is broadly present in tumors. Moreover, because the CBD does not bind to a tumor cell–specific target, it is not subject to clearance by endocytosis or down-regulation of binding due to mutational loss. Hence, the CBD approach turns the tumor stroma matrix into both a drug target and a drug reservoir.

Although the therapeutic effects of CPI and IL-2 in the clinic are remarkable, a number of patients experience serious treatment-related adverse events. In this study, we showed that the incidence of such adverse events caused by CPI and IL-2 therapies was decreased by CBD conjugation or fusion. The reduction of liver and lung toxicity of CPI and reduction of IL-2–induced pulmonary edema by CBD association are especially notable, because those side effects are commonly observed in patients (*10*, *14*). Although the mechanism of the toxicity of tumor immunotherapeutics may be multifactorial,

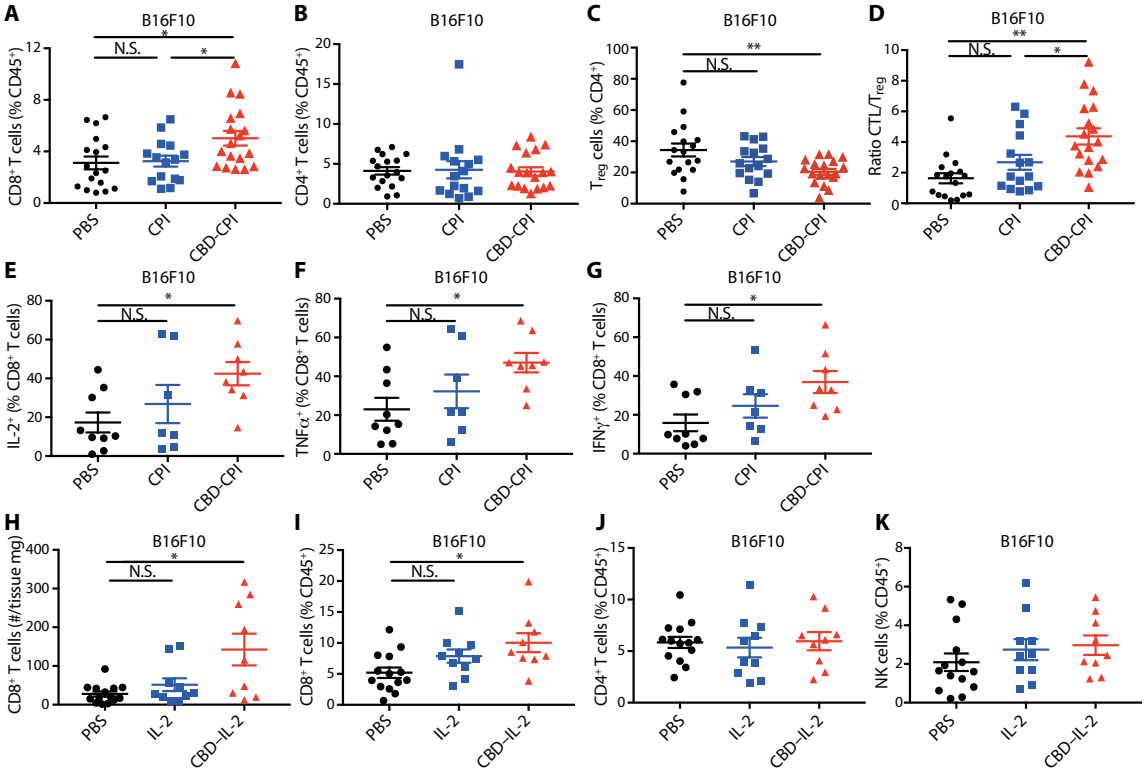

Fig. 4. Both CBD-CPI and CBD–IL-2 treatments increase B16F10 melanoma–infiltrating cytotoxic CD8$^+$T cells. We used the B16F10 model to study T cell behavior in tumors with targeted immunotherapy. B16F10 cells (5×10^5) were inoculated on day 0. CBD-αCTLA4 + CBD–αPD-L1 (CBD-CPI), αCTLA4 + αPD-L1 (CPI), or PBS was administered on day 4. CPI was injected intravenously at 100 μg each. Tumors were collected on day 8, followed by flow cytometric analysis. Frequency of (**A**) $CD8^+CD3^+$ and (**B**) $CD4^+CD3^+$ tumor-infiltrating T cells within $CD45^+$ leukocytes and (**C**) T_{reg} ($Foxp3^+CD25^+$) of $CD4^+CD3^+$ tumor-infiltrating T cells. (**D**) The ratio of CTL ($CD62L^-CD44^+CD8^+CD3^+$) versus T_{reg} ($Foxp3^+CD25^+CD4^+$). (**E** to **G**) T cells were extracted from the tumors and stimulated with αCD28 and αCD3 for 6 hours. Graphs depict the percentage of (E) $IL\text{-}2^+$, (F) $TNF\alpha^+$, and (G) $IFN\gamma^+$ of $CD8^+CD3^+$ T cells. (**H** to **K**) CBD–IL-2, IL-2, or PBS was administered on days 7 to 9. Leukocytes were extracted from the tumor on day 10, followed by flow cytometric analysis. Graphs depict the number of (H) $CD8^+CD3^+$ T cells per tumor weight (mg), the frequency of (I) $CD8^+CD3^+$ T cells within total $CD45^+$ leukocytes, (J) $CD4^+CD3^+$ T cells within total $CD45^+$ leukocytes, and (K) $NK1.1^+CD3^-$ NK cells within total $CD45^+$ leukocytes. Lines represent means ± SEM. Two experimental replicates. Statistical analyses were performed using ANOVA with Tukey's test. Kruskal-Wallis test followed by Dunn's multiple comparison was used in (H) due to nonparametric data. *$P < 0.05$, **$P < 0.01$.

is complicated, and needs detailed future investigation, immunotoxicity in CPI-treated patients is correlated with the concentration of circulating cytokines (*40*). In our previous study, unmodified CPI showed systemic exposure of injected CPI, up-regulation of circulating cytokine concentrations, and liver damage, whereas tumor-localized $PlGF\text{-}2_{123-144}$–CPI did not (*16*). In general, systemic exposure of CPI induces circulating cytokines, which may contribute to tissue damage. CBD conjugation to CPI antibodies and fusion to IL-2 decreased the concentration of the injected drug in the blood by accumulation in the tumor. CBD-CPI did not enhance plasma TNFα concentration, whereas CPI did, which may be one of the mechanisms that contributed to the observed decrease in organ damage. Thus, the decrease in side effects presumably results from competition for the drug by the tumor. Reduction in liver damage was correlated with reduction in $CD8^+$ T cells present in the liver with CBD-CPI treatment compared to unmodified CPI. CBD conjugation to CPI antibody and CBD fusion to IL-2 may even allow decreases in the administered dose, because we observed tumor growth delay at low dosages, where their unmodified forms did not show therapeutic efficacy. These data suggest that CBD drugs may reduce adverse events associated with immunotherapy.

We have observed enhanced antitumor efficacy of both CBD-CPI and CBD–IL-2 compared to their unmodified forms in multiple tumor models. These data suggest that the approach of collagen targeting by the VWF A3 domain is generally applicable to multiple types of solid tumors. EMT6 tumors were less responsive to the CBD-CPI and CBD–IL-2 therapies, suggesting that immune cell recruitment to this immune-excluded tumor is necessary to achieve favorable response to therapy with these pathways.

We observed that systemic injection of CBD-CPI showed similar antitumor efficacy as the local peritumoral administration of $PlGF\text{-}2_{123-144}$–CPI therapy, which is then retained in the tumor injection site through matrix affinity (*16*). CBD-CPI therapy demonstrated clear antitumor immune system activation within the tumor (for example, increased numbers of $CD8^+$ T cells and stimuli-responsive $CD8^+$ T cells), presumably due to increases in the amount of CPI antibody within the tumor, as we observed with CBD–αPD-L1 by imaging analysis. In this study, we tested CBD–αPD-L1, but the use of CBD–αPD-1 may show similar antitumor effects, because the antitumor effect of αPD-L1 and αPD-1 is similar (*41*). CBD-CPI treatment, but not unmodified CPI treatment, decreased the percentage of T_{regs} within the $CD4^+$ T cell population,

supporting the tumor-targeting ability of CBD-αCTLA4, because we used αCTLA4 with T_{reg} depletion capacity (*42*).

IL-2 shows an antitumor effect through inducing proliferation of $CD8^+$ T cells. Thus, with tumor targeting, our data show that CBD–IL-2 increased the numbers of tumor-infiltrating $CD8^+$ T cells compared to unmodified IL-2. We also observed an expansion of intratumoral T_{regs} in some tumor types. Because CBD–IL-2 binds to IL-2Rα (CD25) with a similar affinity to IL-2, we assume that CBD–IL-2 acts on both $CD8^+$ T cells and T_{regs}. Previous reports using Fc-fused IL-2 observed both $CD8^+$ T cell and T_{reg} expansion within B16F10 tumor, concluding that T_{reg} expansion did not affect efficacy of the therapy markedly (*31*). The increased number of $CD8^+$ T cells may be enough to have some antitumor efficacy with the IL-2 therapy, even if T_{reg} number is increased at the same time. Thus, we believe that expansion of $CD8^+$ T cells mainly contributes to the antitumor efficacy of CBD–IL-2.

Because tumor antigen–specific T cells are enriched around tumors (*43*, *44*), CBD-CPI and CBD–IL-2 may effectively activate and expand these T cells, providing superior antitumor efficacy compared to their unmodified forms. CBD-CPI and CBD–IL-2 therapies showed less favorable antitumor effects on the immune-excluded tumor model EMT6, supporting this hypothesis.

The main translational advantage of our approach for tumor-targeted immunotherapy is the systemic delivery route; tumor targeting through CBD association resulted in improvements of both safety and efficacy. CBD–IL-2 can bind to human melanoma sections, consistent with the presence of collagen in the human tumor microenvironment (*30*). For clinical translation of CBD drugs, an advantage lies in the use of a CBD protein that naturally exists in the blood, here, the A3 domain from VWF, limiting the possibility of immune system recognition. In addition, the CBD protein can be conjugated to CPI antibodies with a simple chemical reaction. The advantage of this feature is in simplicity of production, in that it is possible to work with antibodies for which production has already been optimized. The CBD conjugation synthesis reaction for antibodies can be performed in only 90 min using chemistry that is analogous to PEGylation of proteins. This same reaction is used in antibody-drug conjugates, such as in the production of trastuzumab emtansine (*45*). As to CBD–IL-2, given that cytokines are smaller and are generally easy to produce, we chose to recombinantly fuse rather than conjugate the CBD to IL-2. These features may facilitate the development of CBD immunotherapy drugs to overcome the barriers to clinical translation.

One limitation of the CBD-based tumor-targeting approach is that it is only relevant for solid tumors. Moreover, targeting depends on vascular permeability, which may be different in different tumors. For example, it may be difficult to reach tumors that have poor vasculature or limited angiogenesis. In addition, CBD drugs may potentially localize in unfavorable sites, such as wounds, kidney, and liver, where collagen is exposed to components of the bloodstream.

In conclusion, we have developed CBD-conjugated/fused cancer immunotherapy drugs, showing the concept with two structurally different molecular classes, two antibodies, and a cytokine. We found that CBD association enhanced antitumor activity and reduced adverse effects of both αCTLA4 and αPD-L1 combination therapy and IL-2. Our approach demonstrates an interesting methodology (high-affinity protein domains derived from a protein that naturally exists in the blood) and biological approach (targeting a protein that is abundant in the body but that is only exposed in the tumor via its leaky vasculature). This simple approach of an engineered collagen-binding immunotherapy may hold potential for clinical translation as a tumor-targeted immunotherapeutic.

MATERIALS AND METHODS

Study design

This study was designed to test the strategy of targeting immunotherapeutics to tumors through engineered affinity for collagen. Specifically, we tested whether antitumor efficacy and adverse effects of CBD-CPI and CBD–IL-2 against mouse models of melanoma, colon carcinoma, and breast cancer are improved compared to their unmodified forms. We measured tumor growth, the antitumor immune response, and various aspects of toxicity after treatment. These experiments were designed to develop therapeutic strategies to improve the conventional forms of CPI and IL-2 in the clinic. Statistical methods were not used to predetermine necessary sample size, but sample sizes were chosen on the basis of estimates from pilot experiments and previously published results such that appropriate statistical tests could yield statistically significant results. Production of CBD-CPI and CBD–IL-2 was performed by multiple individuals to ensure reproducibility. All experiments were replicated at least twice except for figs. S4, S5, S7, S10, S11 (F to O), and S12 (once). For animal studies, mice were randomized into treatment groups within a cage immediately before the first drug injection and treated in the same manner. Samples were excluded from analysis only when an animal developed a health problem for a nontreatment-related reason, according to the animal care guidelines. The survival end point was reached when the tumor size exceeded 500 mm^3. The *n* values used to calculate statistics are indicated in the figure legends. Drug administration and pathological analyses were performed in a blinded fashion. Statistical methods are described in the "Statistical analysis" section. Original data are located in data file S1.

Production and purification of recombinant VWF A3 domain and IL-2 protein

The sequences encoding the human VWF A3 domain residues Cys^{1670}-Gly^{1874} (907 to 1111 of mature VWF), mouse IL-2, human IL-2, and the fusion of human VWF A3 domain, a $(GGGS)_2$ linker, and mouse IL-2 were synthesized and subcloned into the mammalian expression vector pcDNA3.1(+) by GenScript. A sequence encoding 6×His was added at the N terminus for further purification of the recombinant protein. Suspension-adapted human embryonic kidney–293F cells were routinely maintained in serum-free FreeStyle 293 Expression Medium (Gibco). On the day of transfection, cells were inoculated into fresh medium at a density of 1×10^6 cells/ml. Plasmid DNA (2 μg/ml), linear 25-kDa polyethylenimine (2 μg/ml; Polysciences), and OptiPRO SFM medium (4% final concentration; Thermo Fisher Scientific) were sequentially added. The culture flask was agitated by orbital shaking at 135 rpm at 37°C in the presence of 5% CO_2. Six days after transfection, the cell culture medium was collected by centrifugation and filtered through a 0.22-μm filter. Culture medium was loaded into a HisTrap HP 5 ml column (GE Healthcare), using an ÄKTA pure 25 (GE Healthcare). After washing the column with wash buffer [20 mM imidazole, 20 mM NaH_2PO_4, and 0.5 M NaCl (pH 7.4)], protein was eluted with a gradient of 500 mM imidazole [in 20 mM NaH_2PO_4 and 0.5 M NaCl (pH 7.4)]. The eluate was further purified with size exclusion chromatography using a HiLoad Superdex 200 pg column (GE Healthcare). All purification

steps were carried out at 4°C. The expression of VWF A3 domain was determined by Western blotting using anti–His-tag antibody (BioLegend), and the proteins were verified as >90% pure by SDS-PAGE. Amino acid sequences of produced proteins are shown in table S1.

Synthesis of CBD-CPI antibody

The synthesis was performed as described previously for PlGF-$2_{123–144}$ conjugates (*16*). Rat anti-mouse PD-L1 (clone 10F.9G2, Bio X Cell) and hamster anti-mouse CTLA4 (clone 9H10, Bio X Cell) were incubated with 15 equivalents of sulfosuccinimidyl-4-(*N*-maleimidomethyl) cyclohexane-1-carboxylate (sulfo-SMCC) for 40 min at room temperature (RT). Excess sulfo-SMCC was removed using a Zeba spin desalting column (Thermo Fisher Scientific). More than 10 equivalents of CBD protein (the VWF A3 domain, with a C-terminal cysteine residue) were then added and reacted for 1 hour at RT.

Matrix-assisted laser desorption/ionization–time-of-flight MS

Antibody solutions were purified by size exclusion column chromatograph as described above to exchange the buffer to PBS. Antibodies were analyzed using matrix-assisted laser desorption/ionization–time-of-flight (MALDI-TOF) MS (Bruker UltrafleXtreme MALDI-TOF/TOF). All spectra were collected with acquisition software Bruker flexControl and processed with analysis software Bruker flexAnalysis. First, a saturated solution of the matrix, α-cyano-4-hydroxycinnamic acid (Sigma-Aldrich), was prepared in 50:50 acetonitrile:1% trifluoroacetic acid in water as a solvent. The analyte in PBS (5 μl; 0.1 mg/ml) and the matrix solution (25 μl) were then mixed, and 1 μl of that mixture was deposited on the MTP 384 ground steel target plate. The drop was allowed to dry in a nitrogen gas flow, which resulted in the formation of uniform sample/matrix coprecipitate. All samples were analyzed using high mass linear positive mode method with 2500 laser shots at the laser intensity of 75%. The measurements were externally calibrated at three points with a mix of carbonic anhydrase, phosphorylase B, and bovine serum albumin (BSA).

SDS–polyacrylamide gel electrophoresis

SDS-PAGE was performed as described previously for PlGF-$2_{123–144}$ conjugates (*16*, *46*). SDS-PAGE was performed on 4 to 20% gradient gels (Bio-Rad) after IL-2 was reduced with 10 mM dithiothreitol. After electrophoresis, gels were stained with SimplyBlue SafeStain (Thermo Fisher Scientific) according to the manufacturer's instruction. Gel images were acquired with the ChemiDoc XRS+ system (Bio-Rad).

Detection of CPI antibody binding to collagen and their target proteins

The affinity measurement was performed as described previously for PlGF-$2_{123–144}$ conjugates (*16*, *46*). Ninety-six–well ELISA plates (Greiner Bio-One) were coated with collagen I (10 μg/ml; EMD Millipore), collagen III (EMD Millipore), rmCTLA4 (Sino Biological), or rmPD-L1 (Sino Biological) in PBS for 1 hour at 37°C, followed by blocking with 2% BSA in PBS with 0.05% Tween 20 (PBS-T) for 1 hour at RT. Then, wells were washed with PBS-T and further incubated with CBD-CPI or unmodified CPI (10 μg/ml) for 1 hour at RT. After three washes with PBS-T, wells were incubated for 1 hour at RT with horseradish peroxide (HRP)–conjugated antibody against rat IgG or Syrian hamster IgG (Jackson ImmunoResearch). After washes, bound CPI antibodies were detected with tetramethylbenzidine substrate by measurement of the absorbance at 450 nm with subtraction of the measurement at 570 nm. The apparent K_D values were obtained by nonlinear regression analysis in Prism software (v7, GraphPad Software), assuming one site–specific binding.

Detection of CBD–IL-2 binding to collagen proteins and its receptor

The affinity measurement was performed as described previously for PlGF-$2_{123–144}$ conjugates (*16*, *46*). Ninety-six–well ELISA plates were coated with collagen I (10 μg/ml; EMD Millipore), collagen III (EMD Millipore), or rmIL-2Rα (1 μg/ml; Sino Biological) in PBS for 1 hour at 37°C, followed by blocking with 2% BSA in PBS-T for 1 hour at RT. Then, wells were washed with PBS-T and further incubated with CBD–IL-2 or unmodified IL-2 (10 μg/ml on IL-2 basis) for 1 hour at RT. After three washes with PBS-T, wells were incubated for 1 hour at RT with biotinylated antibody against IL-2 (eBioscience) and then incubated with HRP-conjugated streptavidin (eBioscience) for 1 hour at RT. After washes, bound CBD–IL-2 and IL-2 were detected with tetramethylbenzidine substrate by measurement of the absorbance at 450 nm with subtraction of the measurement at 570 nm. The apparent K_D values were obtained by nonlinear regression analysis in Prism software (v7, GraphPad Software), assuming one site–specific binding.

Proliferation assay

CTLL-2 cells [American Type Culture Collection (ATCC)] were cultured in RPMI 1640 (ATCC), supplemented with 10% heat-inactivated fetal bovine serum (FBS), 2 mM L-glutamine, 1 mM sodium pyruvate, penicillin/streptomycin (100 U/ml), and rmIL-2 (10 ng/ml; Peprotech). Cells were passaged twice a week to a density of 10,000 cells/ml. For proliferation assays, cells were seeded in a 96-well U-bottom cell culture plate at 10,000 cells per well, and mouse IL-2 and CBD–IL-2 were added at indicated concentrations. The concentration of CBD–IL-2 is presented on an IL-2 basis (for example, 1 ng/ml on IL-2 basis, equivalent to 2 ng/ml of CBD–IL-2), in a final volume of 100 μl. Cells were cultured for 48 hours. Cell proliferation was analyzed using the CyQUANT Cell Proliferation Assay Kit (Invitrogen) according to the manufacturer's instructions. Fluorescence was measured using the BioTek Cytation 3 Cell Imaging Multi-Mode Reader (Thermo Fisher Scientific). A dose-response curve was fit via nonlinear regression using Prism software (v7, GraphPad Software).

Human IL-2 binding to PBMCs

Human IL-2 and CBD–human IL-2 were expressed and purified as described above, followed by DyLight 488 (Thermo Fisher Scientific) conjugation, and unreacted dye was removed by a Zeba spin desalting column (Thermo Fisher Scientific) according to the manufacturer's instruction. Protein concentration was determined using a bicinchoninic acid (BCA) assay kit (Thermo Fisher Scientific). PBMCs were purchased from STEMCELL Technologies. A total of 5×10^5 cells per well were seeded in a 96-well microplate. After culturing in RPMI 1640 containing 10% FBS for 2 days, cells were incubated with 1 μg/ml of DyLight 488–labeled IL-2 or equimolar DyLight 488–labeled CBD–IL-2, anti-human CD8, anti-human CD3, and anti-human CD45 antibodies for 60 min on ice. Cells were analyzed by flow cytometry as described below. Obtained mean fluorescence intensity was normalized to the molecular size, considering that CBD–IL-2 showed twice higher fluorescence intensity compared to that of IL-2.

Mice and cell lines

The mice and cell lines were as described previously (*16*, *46*). C57BL/6 and Balb/c mice, age 8 to 15 weeks, were obtained from the Jackson Laboratory. FVB mice, age 8 to 12 weeks, were obtained from Charles River Laboratories. Experiments were performed with approval from the Institutional Animal Care and Use Committee of the University of Chicago. B16F10 cells, CT26 cells, and EMT6 cells were obtained from ATCC and cultured according to the instructions. MMTV-PyMT cells were obtained from spontaneously developed breast cancer in FVB-Tg(MMTV-PyVT) transgenic mice (polyoma middle T antigen oncogene expression was induced by mouse mammary tumor virus promotor) and cultured. All cell lines were checked for mycoplasma contamination by a pathogen test IMPACT I (IDEXX BioResearch).

In vivo biodistribution study

The VWF A3 domain protein was fluorescently labeled using DyLight 800 *N*-hydroxysuccinimide (NHS) ester (Thermo Fisher Scientific), and unreacted dye was removed by a Zebaspin spin column (Thermo Fisher Scientific) according to the manufacturer's instruction. A total of 5×10^5 MMTV-PyMT cells resuspended in 50 μl of PBS were injected subcutaneously into the mammary fat pad on the right side of each FVB mouse. When the tumor reached 500 mm^3, 300 μg of DyLight 800–labeled CBD or equal amount of DyLight 800 dye was injected intravenously 48 hours after injection, and mice were euthanized and were perfused transcardially with 10 ml of PBS. Organs (heart, lung, stomach, tumor, kidney, spleen, and liver) were extracted and imaged with the IVIS Imaging System 100 (Xenogen) under the following conditions: f/stop, 2; optical filter excitation, 745 nm; emission, 800 nm; exposure time, 1 s; small binning. Signals of the VWF A3 domain (CBD) proteins were obtained by subtracting signals of DyLight 800 dye from signals of DyLight 800 CBD protein in each organ. The percentage of distribution of CBD protein in each organ was determined by signals of CBD protein in each organ/total signals of CBD protein × 100.

Histological analysis of injected CBD–αPD-L1 within tumor

αPD-L1 (clone 10F.9G2, Bio X cell) and αCD31 (clone MEC13.3, BioLegend) were purchased. CBD–αPD-L1 was synthesized and purified as described above. The antibodies were conjugated to DyLight 594 or 633 NHS fluorescent dyes (Thermo Fisher Scientific) at antibody/dye molecule molar ratio of 1:30. Reactions were incubated with gentle agitation at 4°C overnight, followed by dialysis in 10-kDa molecular weight cutoff Slide-A-Lyzer cassettes (Thermo Fisher Scientific) against PBS (pH 7.4) at 4°C for 3 days. Fluorescent antibody solutions were stored at 4°C. DyLight 594–αPD-L1 (100 μg) or DyLight 594–CBD–αPD-L1 (100 μg) was intravenously injected into MMTV-PyMT tumor–bearing mice. Thirty minutes after injection (when the majority of αPD-L1 was not internalized into cells), tumors were harvested and prepared for microscopy as previously described (*47*). Briefly, tumor tissues were washed with cold PBS, fixed with 2% paraformaldehyde in PBS for 10 min at RT, and washed with PBS. Then, tumors were cast in 2% agarose gel (dissolved in distilled water; LE Quick Dissolve Agarose, GeneMate) in 24-well plates. The gel plugs containing tumors were mounted on a vibrating microtome (VT1200S, Leica) equipped with a buffer tray. Sections (0.4 mm in thickness) were collected in cold PBS. The macrosections were stained with DyLight 633–αCD31 in staining buffer [RPMI 1640 medium with BSA (10 mg/ml) and 0.1% Triton X-100] at 4°C overnight. The macrosections were incubated sequentially in 10 ml of 20, 50, and 80% (w/v) D-fructose solution for 30 min, 1 hour, and 1 hour, respectively, at 25°C with gentle agitation in 20-ml glass vials. A Leica TCS SP8 confocal laser scanning microscope, a white light laser, and a Leica HCX PL APO 10×/0.4 numerical aperture dry objective (2.2-mm working distance) were used for imaging with 594-nm excitation and 600- to 620-nm filters for DyLight 594, and 633-nm excitation and 637- to 655-nm filters for DyLight 633. All image analyses were conducted with basic functions in Fiji software. We visually determined the cutoff threshold for the antibodies and CD31 channel images and converted into binary (8-bit) images. The tumor area was determined by outlining tumor boundary in the image data. To measure the distance of antibody from $CD31^+$ tumor vasculature, we applied a distance map to the tumor blood vessel images.

CBD–IL-2 binding to human melanoma tissue

Human melanoma frozen tissue sections were purchased from OriGene Technologies. The tissues were blocked with 2% BSA in PBS-T for 1 hour at RT. Tissue was incubated with 25 μg/ml of mouse IL-2 or equimolar CBD–mouse IL-2 in PBS-T for 2 hours at RT. The tissues were stained with hamster anti-human CD31 antibody (Abcam), goat anti-mouse IL-2 antibody (R&D systems), and rabbit anti–collagen I antibody (Abcam) for 1 hour at RT. After staining with the fluorescently tagged secondary antibodies, slides were covered with ProLong Gold Antifade Mountant with DAPI (Thermo Fisher Scientific). An IX83 microscope (Olympus) was used for imaging. Images were processed using ImageJ software (National Institutes of Health).

Blood concentration analysis of injected CPI and IL-2

The blood concentration analysis for CPI was performed as described previously (*16*). B16F10 melanoma cells (5×10^5) were injected intradermally on the left side of the back of each mouse. IL-2 and CBD–IL-2 were fluorescently tagged using DyLight 800 NHS (Thermo Fisher Scientific) according to the manufacturer's instruction. After 4 days, mice were injected intravenously with 100 μg each of CPI. Blood samples were collected in protein low-binding tubes (Eppendorf) on 1, 2, 4, and 6 days after CPI injection, followed by >4-hour incubation at 4°C. After 7 days, 21 μg of IL-2 or CBD–IL-2 (30 μg on IL-2 basis, equivalent to 60 μg of CBD–IL-2) was injected intravenously. For IL-2, blood samples were collected in EDTA-containing heparinized tubes 1 and 10 min after IL-2 injection. Concentrations of CPI in serum were measured by ELISA as described above. Concentrations of IL-2 in plasma were measured with a LI-COR Infrared Odyssey Imager. Plasma half-life was estimated by a simple linear regression model using Prism software (v7, GraphPad Software).

Serum cytokine concentration analysis

The serum cytokine concentration analysis was performed as described previously (*16*). B16F10 melanoma cells (5×10^5) were injected intradermally on the left side of the back of each 15-week-old C57BL/6 mouse. After 4 and 7 days, mice received two doses of CBD-CPI or unmodified CPI (αPD-L1 and αCTLA4; 100 μg each) intravenously. Blood samples were collected in protein low-binding tubes (Eppendorf) on day 8, followed by overnight incubation at 4°C. Cytokine concentrations in serum were measured by Ready-SET-Go! ELISA kits (eBioscience) according to the manufacturer's protocol.

ALT and AST activity analysis

The liver damage marker analysis was performed as described previously (*16*, *46*). B16F10 tumor–bearing mice received CPI injection (αPD-L1 and αCTLA4; 100 μg each) 4 and 7 days after tumor inoculation. On day 10, blood samples were collected in tubes, followed by >4-hour incubation at 4°C. On the same day, serum was collected, and ALT and AST activities were measured by an ALT assay kit or an AST assay kit (both from Sigma-Aldrich) according to the manufacturer's protocol.

CPI treatment effect on liver water content

B16F10 tumor–bearing mice received CPI injection (αPD-L1 and αCTLA4; 100 μg each) 4 and 7 days after tumor inoculation. On day 10, the liver was harvested and weighed. Water content in the liver was determined by weighing before and after overnight lyophilization using FreeZone 6 Benchtop Freeze Dryer (Labconco).

Liver leukocyte analysis after CPI treatment

B16F10 tumor–bearing mice received CPI injection (αPD-L1 and αCTLA4; 100 μg each) 4 and 7 days after tumor inoculation. On day 10, the liver was harvested and digested, followed by flow cytometric analysis described below.

Liver, lung, and kidney histology

The histological analysis was performed as described previously (*16*, *46*). B16F10 tumor–bearing mice received CBD-CPI or unmodified CPI injection (αPD-L1 and αCTLA4; 100 μg each) 4 and 7 days after tumor inoculation. Ten days after tumor inoculation, mice were euthanized with CO_2 inhalation. Then, the liver, lung, and kidney were collected and fixed with 2% paraformaldehyde. After embedding in paraffin, blocks were cut into 5-μm sections, followed by staining with hematoxylin and eosin. Images were captured with an EVOS FL Auto microscope (Life Technologies). For quantification of leukocytic infiltration, the number of leukocyte infiltration foci in 10 high-power fields (×400) was counted with light microscopy (BX53, Olympus). Slides were evaluated independently by two pathologists (H.A. and M.Y.) who were blinded to the treatment grouping. Microscopic images were captured with color charge-coupled device camera (DP27, Olympus).

The IL-2 treatment effect on lung and spleen

A total of 5×10^5 B16F10 cells resuspended in 50 μl of PBS were inoculated intradermally on the left side of the back of each C57BL/6 mouse on day 0. IL-2 (6 μg) or CBD–IL-2 (6 μg on IL-2 basis, equivalent to 12 μg of CBD–IL-2) was injected intravenously on days 7 to 9. On day 10, spleen and lung were harvested and weighed. Water content in the lung was determined by weighing before and after overnight lyophilization using FreeZone 6 Benchtop Freeze Dryer (Labconco).

Antitumor efficacy of CPI and IL-2 on B16F10 tumor

The measurement of antitumor efficacy was performed as described previously for PlGF-$2_{123–144}$ conjugates (*16*, *46*). A total of 5×10^5 B16F10 cells resuspended in 50 μl of PBS were inoculated intradermally on the left side of the back of each C57BL/6 mouse. After 4 days, mice were injected with CBD-CPI or unmodified CPI (αPD-L1 and αCTLA4; 25 or 100 μg each), IL-2 (6 μg), or CBD–IL-2 (6 μg on IL-2 basis, equivalent to 12 μg of CBD–IL-2). PlGF-$2_{123–144}$–conjugated CPI (αPD-L1 and αCTLA4; 100 μg each) was prepared and injected peritumorally as described previously (*16*). Tumors were measured with a digital caliper starting 4 days after tumor inoculation, and volumes were calculated as ellipsoids, where $V = 4/3 \times 3.14 \times \text{depth}/2 \times \text{width}/2 \times \text{height}/2$. Mice were euthanized at the point when tumor volume had reached over 500 mm^3.

Antitumor efficacy of CPI and IL-2 on CT26 tumor

The measurement of antitumor efficacy was performed as described previously for PlGF-$2_{123–144}$ conjugates (*46*). A total of 5×10^5 CT26 cells resuspended in 50 μl of PBS were inoculated intradermally on the left side of the back of each Balb/c mouse. After 5 days, mice were injected intravenously with CBD-CPI or unmodified CPI (αPD-L1 and αCTLA4; 25 or 100 μg each), IL-2 (6 μg), or CBD–IL-2 (6 μg on IL-2 basis, equivalent to 12 μg of CBD–IL-2). Tumors were measured with a digital caliper starting 5 days after tumor inoculation as described above. Mice were euthanized at the point when tumor volume had reached over 500 mm^3.

Antitumor efficacy of CPI, IL-2, and CPI + IL-2 combination on MMTV-PyMT tumor

The measurement of antitumor efficacy was performed as described previously for PlGF-$2_{123–144}$ conjugates (*16*, *46*). A total of 5×10^5 MMTV-PyMT cells resuspended in 50 μl of PBS were injected subcutaneously into the mammary gland on the right side of each FVB mouse. After 7 days, mice were injected intravenously with CPI (αPD-L1 and αCTLA4; 100 μg each), IL-2 (6 μg), or CBD–IL-2 (6 μg on IL-2 basis, equivalent to 12 μg of CBD–IL-2). For combination therapy of CPI and IL-2, CPI (αPD-L1 and αCTLA4; 25 μg each) and IL-2 (6 μg) were administered on days 7, 14, and 21. Tumors were measured with a digital caliper as described above. Mice were euthanized when tumor volume reached over 500 mm^3. For tumor rechallenge, 30 days after the first tumor inoculation in the right mammary gland fat pad, 5×10^5 MMTV-PyMT cells were inoculated into the left mammary gland fat pad in CBD-CPI–treated tumor-free survivors or in naïve mice.

Antitumor efficacy of CPI and IL-2 on EMT6 tumor

A total of 5×10^5 EMT6 cells resuspended in 50 μl of PBS were inoculated subcutaneously into the mammary gland on the right side of each Balb/c mouse. Mice were injected intravenously with CBD-CPI or unmodified CPI (αPD-L1 and αCTLA4; 100 μg each) on days 7 and 10. IL-2 (6 μg), or CBD–IL-2 (6 μg on IL-2 basis, equivalent to 12 μg of CBD–IL-2) were injected on days 7, 10, and 13. Tumors were measured with a digital caliper starting 7 days after tumor inoculation as described above. Mice were euthanized at the point when tumor volume had reached over 500 mm^3.

Tissue and cell preparation and immune cell subset analysis

The immune cell subset analysis was performed as described previously (*16*). B16F10 melanoma cells (5×10^5) were injected intradermally on the left side of the back of each C57BL/6 mouse. A total of 1×10^6 MMTV-PyMT cells or 5×10^5 EMT6 cells were inoculated subcutaneously into the mammary gland on the right side of each FVB mouse or Balb/c mouse, respectively. Mice were injected intravenously with CPI (αPD-L1 and αCTLA4; 100 μg each) on day 4, or with IL-2 (6 μg) on days 7 to 9 (B16F10) on two consecutive days after tumor size reached 50 mm^3 (MMTV-PyMT), or on days 7 and 8 (EMT6). B16F10 tumor–bearing mice were euthanized on day 8 (CPI T/NK cell analysis), day 10 (CPI MDSC analysis), or day 10 (IL-2).

MMTV-PyMT tumor–bearing mice were euthanized 1 day after the second injection. EMT6 tumor–bearing mice were euthanized on day 9. The tumors, livers, and spleens were harvested and were digested in Dulbecco's modified Eagle's medium, supplemented with 2% FBS, collagenase D (2 mg/ml), and deoxyribonuclease I (40 μg/ml; Roche) for 30 min at 37°C. Single-cell suspensions were obtained by gently disrupting the liver, spleen, and enzyme-treated tumor through a 70-μm cell strainer. Red blood cells were lysed with ACK lysing buffer (Quality Biological). Cells were counted and resuspended in Iscove's modified Dulbecco's medium, supplemented with 10% FBS and 1% penicillin/streptomycin (full medium; all from Life Technologies), and used for flow cytometry staining.

Ex vivo T cell stimulation

The ex vivo T cell stimulation was performed as described previously (*16*). Single-cell suspensions from tumor were prepared as described above. $CD8^+$ T cells were isolated using EasySep kits (STEMCELL Technologies) following the manufacturer's instructions, except that biotinylated αCD105 (12403, BioLegend) was added to the EasySep $CD8^+$ T cell Isolation Cocktail to remove B16F10 melanoma cells. Ninety-six–well cell culture plates (BD Falcon) were coated with αCD3 (10 μg/ml; 145-2C11, BioLegend) in PBS overnight at 37°C. Extracted T cells from tumors were plated in 96-well plates and cultured in full medium for 6 hours at 37°C in the presence of αCD28 (2 μg/ml; EL-4, BioLegend) and brefeldin A (5 μg/ml; Sigma-Aldrich). Cells were harvested, stained, and analyzed by flow cytometry as described below.

Flow cytometry and antibodies

The flow cytometric analysis was performed as described previously (*16*). Single-cell suspensions from tissues were prepared as described above. Antibodies against the following molecules were used throughout the paper if not otherwise indicated: anti-mouse CD3 (145-2C11, BD Biosciences), anti-human CD3 (UCHT1, BD Pharmingen), CD4 (RM4-5, BD Biosciences), anti-mouse CD8α (53-6.7, BD Biosciences), anti-human CD8α (SK1, BioLegend), CD25 (PC61, BD Biosciences), anti-mouse CD45 (30-F11, BD Biosciences), anti-human CD45 (2D1, eBioscience), CD44 (IM7, BD Biosciences), CD62L (MEL-14, BD Biosciences), PD-1 (29F.1A12, BD Biosciences), NK1.1 (PK136, BD Biosciences), Foxp3 (MF23, BD Biosciences), F4/80 (T45-2342, BD Biosciences), MHCII (M5/114.15.2, BioLegend), Ly6G (1A8, BioLegend), Ly6C (HK1.4, BioLegend), CD11b (M1/70, BioLegend), CD11c (HL3, BD Biosciences), B220 (RA3-6B2, BioLegend), IL-2 (JES6-5H4, BD Biosciences), IFNγ (XMG1.2, BD Biosciences), and TNFα (MP6-XT22, eBioscience). Fixable live/dead cell discrimination was performed using Fixable Viability Dye eFluor 455 (eBioscience) according to the manufacturer's instructions. Staining was carried out on ice for 20 min if not indicated otherwise, and intracellular staining was performed using the Foxp3 staining kit (BioLegend) according to the manufacturer's instructions. After a washing step, cells were stained with specific antibodies for 20 min on ice before fixation. All flow cytometric analyses were performed using a LSRFortessa flow cytometer (BD Biosciences) and analyzed using FlowJo software (Tree Star).

Statistical analysis

The statistical significance of differences between experimental groups was assessed using Prism software (v7, GraphPad Software). Where one-way ANOVA followed by Tukey's post hoc test was used, variance between groups was found to be similar by Brown-Forsythe test. For nonparametric data, Kruskal-Wallis test followed by Dunn's multiple comparison test was used. For single comparisons, a two-tailed Student's *t* test was used. Survival curves were analyzed using the log-rank (Mantel-Cox) test.

SUPPLEMENTARY MATERIALS

www.sciencetranslationalmedicine.org/cgi/content/full/11/487/eaau3259/DC1
Fig. S1. Molecular weights are increased by CBD conjugation to αPD-L1 or fusion to IL-2.
Fig. S2. Affinities of CBD-αCTLA4, CBD–αPD-L1, and CBD–IL-2 for collagen I and III and their target proteins were determined.
Fig. S3. Both CBD–IL-2 and IL-2 proliferate and bind target cells.
Fig. S4. Distribution of CBD–αPD-L1 and αPD-L1 within the tumor was analyzed.
Fig. S5. Blood concentrations of injected CBD-CPI, CBD–IL-2, and their unmodified forms were analyzed.
Fig. S6. Leukocyte infiltration in the liver, lung, and kidney after unmodified CPI and CBD-CPI treatment was analyzed.
Fig. S7. Populations of leukocytes infiltrated into the liver after unmodified CPI or CBD-CPI treatment were analyzed.
Fig. S8. Conjugation of CBD to CPI is indispensable for B16F10 tumor growth suppression.
Fig. S9. EMT6 immune-excluded tumor is not very responsive to CBD-CPI and CBD–IL-2.
Fig. S10. CBD-CPI treatment decreases immunosuppressive MDSCs within B16F10 tumor.
Fig. S11. Immune cells within B16F10 tumor and spleen were analyzed after CBD–IL-2 treatment.
Fig. S12. CBD–IL-2 treatment increases the number of $CD8^+$ T cells and NK cells within MMTV-PyMT tumor but not within EMT6 tumor.
Table S1. Protein sequences.
Data file S1. Original data.

REFERENCES AND NOTES

1. J. P. Allison, Immune checkpoint blockade in cancer therapy: The 2015 Lasker-DeBakey clinical medical research award. *JAMA* **314**, 1113–1114 (2015).
2. P. Sharma, J. P. Allison, The future of immune checkpoint therapy. *Science* **348**, 56–61 (2015).
3. S. L. Topalian, C. G. Drake, D. M. Pardoll, Immune checkpoint blockade: A common denominator approach to cancer therapy. *Cancer Cell* **27**, 450–461 (2015).
4. J. F. Grosso, M. N. Jure-Kunkel, CTLA-4 blockade in tumor models: An overview of preclinical and translational research. *Cancer Immun.* **13**, 5 (2013).
5. F. S. Hodi, S. J. O'Day, D. F. McDermott, R. W. Weber, J. A. Sosman, J. B. Haanen, R. Gonzalez, C. Robert, D. Schadendorf, J. C. Hassel, W. Akerley, A. J. M. van den Eertwegh, J. Lutzky, P. Lorigan, J. M. Vaubel, G. P. Linette, D. Hogg, C. H. Ottensmeier, C. Lebbé, C. Peschel, I. Quirt, J. I. Clark, J. D. Wolchok, J. S. Weber, J. Tian, M. J. Yellin, G. M. Nichol, A. Hoos, W. J. Urba, Improved survival with ipilimumab in patients with metastatic melanoma. *N. Engl. J. Med.* **363**, 711–723 (2010).
6. J. R. Brahmer, S. S. Tykodi, L. Q. M. Chow, W.-J. Hwu, S. L. Topalian, P. Hwu, C. G. Drake, L. H. Camacho, J. Kauh, K. Odunsi, H. C. Pitot, O. Hamid, S. Bhatia, R. Martins, K. Eaton, S. Chen, T. M. Salay, S. Alaparthy, J. F. Grosso, A. J. Korman, S. M. Parker, S. Agrawal, S. M. Goldberg, D. M. Pardoll, A. Gupta, J. M. Wigginton, Safety and activity of anti-PD-L1 antibody in patients with advanced cancer. *N. Engl. J. Med.* **366**, 2455–2465 (2012).
7. H. O. Alsaab, S. Sau, R. Alzhrani, K. Tatiparti, K. Bhise, S. K. Kashaw, A. K. Iyer, PD-1 and PD-L1 checkpoint signaling inhibition for cancer immunotherapy: Mechanism, combinations, and clinical outcome. *Front. Pharmacol.* **8**, 561 (2017).
8. J. Larkin, V. Chiarion-Sileni, R. Gonzalez, J. J. Grob, C. L. Cowey, C. D. Lao, D. Schadendorf, R. Dummer, M. Smylie, P. Rutkowski, P. F. Ferrucci, A. Hill, J. Wagstaff, M. S. Carlino, J. B. Haanen, M. Maio, I. Marquez-Rodas, G. A. McArthur, P. A. Ascierto, G. V. Long, M. K. Callahan, M. A. Postow, K. Grossmann, M. Sznol, B. Dreno, L. Bastholt, A. Yang, L. M. Rollin, C. Horak, F. S. Hodi, J. D. Wolchok, Combined nivolumab and ipilimumab or monotherapy in untreated melanoma. *N. Engl. J. Med.* **373**, 23–34 (2015).
9. C. Boutros, A. Tarhini, E. Routier, O. Lambotte, F. L. Ladurie, F. Carbonnel, H. Izzeddine, A. Marabelle, S. Champiat, A. Berdelou, E. Lanoy, M. Texier, C. Libenciuc, A. M. M. Eggermont, J.-C. Soria, C. Mateus, C. Robert, Safety profiles of anti-CTLA-4 and anti-PD-1 antibodies alone and in combination. *Nat. Rev. Clin. Oncol.* **13**, 473–486 (2016).
10. M. A. Postow, R. Sidlow, M. D. Hellmann, Immune-related adverse events associated with immune checkpoint blockade. *N. Engl. J. Med.* **378**, 158–168 (2018).
11. O. Boyman, J. Sprent, The role of interleukin-2 during homeostasis and activation of the immune system. *Nat. Rev. Immunol.* **12**, 180–190 (2012).
12. T. Jiang, C. Zhou, S. Ren, Role of IL-2 in cancer immunotherapy. *Oncoimmunology* **5**, e1163462 (2016).

13. S. A. Rosenberg, J. C. Yang, S. L. Topalian, D. J. Schwartzentruber, J. S. Weber, D. R. Parkinson, C. A. Seipp, J. H. Einhorn, D. E. White, Treatment of 283 consecutive patients with metastatic melanoma or renal cell cancer using high-dose bolus interleukin 2. *JAMA* **271**, 907–913 (1994).
14. S. A. Rosenberg, M. T. Lotze, L. M. Muul, S. Leitman, A. E. Chang, S. E. Ettinghausen, Y. L. Matory, J. M. Skibber, E. Shiloni, J. T. Vetto, C. A. Seipp, C. Simpson, C. M. Reichert, Observations on the systemic administration of autologous lymphokine-activated killer cells and recombinant interleukin-2 to patients with metastatic cancer. *N. Engl. J. Med.* **313**, 1485–1492 (1985).
15. J. A. Klapper, S. G. Downey, F. O. Smith, J. C. Yang, M. S. Hughes, U. S. Kammula, R. M. Sherry, R. E. Royal, S. M. Steinberg, S. Rosenberg, High-dose interleukin-2 for the treatment of metastatic renal cell carcinoma: A retrospective analysis of response and survival in patients treated in the surgery branch at the National Cancer Institute between 1986 and 2006. *Cancer* **113**, 293–301 (2008).
16. J. Ishihara, K. Fukunaga, A. Ishihara, H. M. Larsson, L. Potin, P. Hosseinchi, G. Galliverti, M. A. Swartz, J. A. Hubbell, Matrix-binding checkpoint immunotherapies enhance antitumor efficacy and reduce adverse events. *Sci. Transl. Med.* **9**, eaan0401 (2017).
17. S. Ricard-Blum, The collagen family. *Cold Spring Harb. Perspect. Biol.* **3**, a004978 (2011).
18. C. Dubois, L. Panicot-Dubois, G. Merrill-Skoloff, B. Furie, B. C. Furie, Glycoprotein VI–dependent and –independent pathways of thrombus formation in vivo. *Blood* **107**, 3902–3906 (2006).
19. W. Bergmeier, R. O. Hynes, Extracellular matrix proteins in hemostasis and thrombosis. *Cold Spring Harb. Perspect. Biol.* **4**, a005132 (2012).
20. J. A. Nagy, S.-H. Chang, A. M. Dvorak, H. F. Dvorak, Why are tumour blood vessels abnormal and why is it important to know? *Br. J. Cancer* **100**, 865–869 (2009).
21. H. Liang, X. Li, B. Chen, B. Wang, Y. Zhao, Y. Zhuang, H. Shen, Z. Zhang, J. Dai, A collagen-binding EGFR single-chain Fv antibody fragment for the targeted cancer therapy. *J. Control. Release* **209**, 101–109 (2015).
22. H. Liang, X. Li, B. Wang, B. Chen, Y. Zhao, J. Sun, Y. Zhuang, J. Shi, H. Shen, Z. Zhang, J. Dai, A collagen-binding EGFR antibody fragment targeting tumors with a collagen-rich extracellular matrix. *Sci. Rep.* **6**, 18205 (2016).
23. S. Sabrkhany, A. W. Griffioen, M. G. A. Oude Egbrink, The role of blood platelets in tumor angiogenesis. *Biochim. Biophys. Acta* **1815**, 189–196 (2011).
24. Z.-H. Zhou, C.-D. Ji, H.-L. Xiao, H.-B. Zhao, Y.-H. Cui, X.-W. Bian, Reorganized collagen in the tumor microenvironment of gastric cancer and its association with prognosis. *J. Cancer* **8**, 1466–1476 (2017).
25. P. P. Provenzano, D. R. Inman, K. W. Eliceiri, J. G. Knittel, L. Yan, C. T. Rueden, J. G. White, P. J. Keely, Collagen density promotes mammary tumor initiation and progression. *BMC Med.* **6**, 11 (2008).
26. M. Shahidi, Thrombosis and von Willebrand factor. *Adv. Exp. Med. Biol.* **906**, 285–306 (2017).
27. C. Addi, F. Murschel, G. De Crescenzo, Design and use of chimeric proteins containing a collagen-binding domain for wound healing and bone regeneration. *Tissue Eng. Part B Rev.* **2**, 163–182 (2016).
28. A. S. Ribba, I. Loisel, J. M. Lavergne, I. Juhan-Vague, B. Obert, G. Cherel, D. Meyer, J. P. Girma, Ser968Thr mutation within the A3 domain of von Willebrand factor (VWF) in two related patients leads to a defective binding of VWF to collagen. *Thromb. Haemost.* **86**, 848–854 (2001).
29. B. K. Ballmer-Weber, R. Dummer, E. Küng, G. Burg, P. E. Ballmer, Interleukin 2-induced increase of vascular permeability without decrease of the intravascular albumin pool. *Br. J. Cancer* **71**, 78–82 (1995).
30. S. Mariathasan, S. J. Turley, D. Nickles, A. Castiglioni, K. Yuen, Y. Wang, E. E. Kadel III, H. Koeppen, J. L. Astarita, R. Cubas, S. Jhunjhunwala, R. Banchereau, Y. Yang, Y. Guan, C. Chalouni, J. Ziai, Y. Şenbabaoğlu, S. Santoro, D. Sheinson, J. Hung, J. M. Giltnane, A. A. Pierce, K. Mesh, S. Lianoglou, J. Riegler, R. A. D. Carano, P. Eriksson, M. Höglund, L. Somarriba, D. L. Halligan, M. S. van der Heijden, Y. Loriot, J. E. Rosenberg, L. Fong, I. Mellman, D. S. Chen, M. Green, C. Derleth, G. D. Fine, P. S. Hegde, R. Bourgon, T. Powles, TGFβ attenuates tumour response to PD-L1 blockade by contributing to exclusion of T cells. *Nature* **554**, 544–548 (2018).
31. E. F. Zhu, S. A. Gai, C. F. Opel, B. H. Kwan, R. Surana, M. C. Mihm, M. J. Kauke, K. D. Moynihan, A. Angelini, R. T. Williams, M. T. Stephan, J. S. Kim, M. B. Yaffe, D. J. Irvine, L. M. Weiner, G. Dranoff, K. D. Wittrup, Synergistic innate and adaptive immune response to combination immunotherapy with anti-tumor antigen antibodies and extended serum half-life IL-2. *Cancer Cell* **27**, 489–501 (2015).
32. S. A. Quezada, K. S. Peggs, M. A. Curran, J. P. Allison, CTLA4 blockade and GM-CSF combination immunotherapy alters the intratumor balance of effector and regulatory T cells. *J. Clin. Invest.* **116**, 1935–1945 (2006).
33. F. Danhier, O. Feron, V. Préat, To exploit the tumor microenvironment: Passive and active tumor targeting of nanocarriers for anti-cancer drug delivery. *J. Control. Release* **148**, 135–146 (2010).
34. B. Carnemolla, L. Borsi, E. Balza, P. Castellani, R. Meazza, A. Berndt, S. Ferrini, H. Kosmehl, D. Neri, L. Zardi, Enhancement of the antitumor properties of interleukin-2 by its targeted delivery to the tumor blood vessel extracellular matrix. *Blood* **99**, 1659–1665 (2002).
35. D. W. Kufe, MUC1-C oncoprotein as a target in breast cancer: Activation of signaling pathways and therapeutic approaches. *Oncogene* **32**, 1073–1081 (2013).
36. J.-P. Mach, F. Buchegger, M. Forni, J. Ritschard, C. Berche, J.-D. Lumbroso, M. Schreyer, C. Girardet, R. S. Accolla, S. Carrel, Use of radiolabelled monoclonal anti-CEA antibodies for the detection of human carcinomas by external photoscanning and tomoscintigraphy. *Immunol. Today* **2**, 239–249 (1981).
37. P. Busek, R. Mateu, M. Zubal, L. Kotackova, A. Sedo, Targeting fibroblast activation protein in cancer - prospects and caveats. *Front. Biosci.* **23**, 1933–1968 (2018).
38. H. Maeda, J. Wu, T. Sawa, Y. Matsumura, K. Hori, Tumor vascular permeability and the EPR effect in macromolecular therapeutics: A review. *J. Control. Release* **65**, 271–284 (2000).
39. M. A. Swartz, M. E. Fleury, Interstitial flow and its effects in soft tissues. *Annu. Rev. Biomed. Eng.* **9**, 229–256 (2007).
40. S. Y. Lim, J. H. Lee, T. N. Gide, A. M. Menzies, A. Guminski, M. S. Carlino, E. J. Breen, J. Y. H. Yang, S. Ghazanfar, R. F. Kefford, R. A. Scolyer, G. V. Long, H. Rizos, Circulating cytokines predict immune-related toxicity in melanoma patients receiving anti-PD-1–based immunotherapy. *Clin. Cancer Res.* **25**, 1557–1563 (2019).
41. R. N. Pillai, M. Behera, T. K. Owonikoko, A. O. Kamphorst, S. Pakkala, C. P. Belani, F. R. Khuri, R. Ahmed, S. S. Ramalingam, Comparison of the toxicity profile of PD-1 versus PD-L1 inhibitors in non-small cell lung cancer: A systematic analysis of the literature. *Cancer* **124**, 271–277 (2018).
42. T. R. Simpson, F. Li, W. Montalvo-Ortiz, M. A. Sepulveda, K. Bergerhoff, F. Arce, C. Roddie, J. Y. Henry, H. Yagita, J. D. Wolchok, K. S. Peggs, J. V. Ravetch, J. P. Allison, S. A. Quezada, Fc-dependent depletion of tumor-infiltrating regulatory T cells co-defines the efficacy of anti–CTLA-4 therapy against melanoma. *J. Exp. Med.* **210**, 1695–1710 (2013).
43. S. Hadrup, M. Donia, P. Thor Straten, Effector CD4 and CD8 T cells and their role in the tumor microenvironment. *Cancer Microenviron.* **6**, 123–133 (2013).
44. M. T. Bethune, A. V. Joglekar, Personalized T cell-mediated cancer immunotherapy: Progress and challenges. *Curr. Opin. Biotechnol.* **48**, 142–152 (2017).
45. J. M. Lambert, R. V. J. Chari, Ado-trastuzumab Emtansine (T-DM1): An antibody-drug conjugate (ADC) for HER2-positive breast cancer. *J. Med. Chem.* **57**, 6949–6964 (2014).
46. J. Ishihara, A. Ishihara, L. Potin, P. Hosseinchi, K. Fukunaga, M. Damo, T. F. Gajewski, M. A. Swartz, J. A. Hubbell, Improving efficacy and safety of agonistic anti-CD40 antibody through extracellular matrix affinity. *Mol. Cancer Ther.* **17**, 2399–2411 (2018).
47. S. S. Lee, V. P. Bindokas, S. J. Kron, Multiplex three-dimensional optical mapping of tumor immune microenvironment. *Sci. Rep.* **7**, 17031 (2017).

Acknowledgments: We thank the Human Tissue Resource Center of the University of Chicago for histology analysis. We thank A. Solanki for assistance in tail vein injections and S. Gomes for experimental help. **Funding:** This work was supported by the European Research Commission grant Cytrix (to J.A.H.). This work was supported in part by National Cancer Institute R01 CA199663 (to S.J.K.) and by National Institute of Biomedical Imaging and Bioengineering K99 EB022636 (to S.S.-Y.L.). K.S. is supported by Research Fellowship for Young Scientists (JSPS, JP17J05032) and Advanced Graduate Course on Molecular Systems for Devices (Kyushu University). L.P. is funded by the Fonds Pierre-François Vittone. **Author contributions:** J.I., A.I., M.A.S., and J.A.H. designed the project. J.I. and A.I. performed experiments. J.I., A.I., and J.A.H. analyzed data. J.I., A.I., and J.A.H. wrote the paper. K.S., J.-M.W., L.P., P.H., K.F., L.T.G., A.M., and K.K. assisted with tumor experiments. M.M.R. assisted with protein MS. S.S.-Y.L., and S.J.K. assisted with imaging analysis. M.Y., H.A., and M.F. performed the histopathological analysis. **Competing interests:** J.I., A.I, K.S., K.F., M.A.S., and J.A.H. are inventors on U.S. Provisional Patent applications 62/638,520, 28/984,351, and 62/727,156. J.I., A.I., M.A.S., and J.A.H. are founders and shareholders in Arrow Immune Inc., which is developing the technology presented in this report, and J.A.H. and M.A.S. have leadership roles in that company. S.S.-Y.L. and S.J.K. have founded Transnostics to commercialize tumor imaging methods used here. K.F. is currently affiliated with FUJIFILM Corporation (Kanagawa, Japan). The other authors declare that they have no competing interests. **Data and materials availability:** All data associated with this study are present in the paper or the Supplementary Materials.

Submitted 4 June 2018
Resubmitted 27 November 2018
Accepted 22 February 2019
Published 10 April 2019
10.1126/scitranslmed.aau3259

Citation: J. Ishihara, A. Ishihara, K. Sasaki, S. S.-Y. Lee, J.-M. Williford, M. Yasui, H. Abe, L. Potin, P. Hosseinchi, K. Fukunaga, M. M. Raczy, L. T. Gray, A. Mansurov, K. Katsumata, M. Fukayama, S. J. Kron, M. A. Swartz, J. A. Hubbell, Targeted antibody and cytokine cancer immunotherapies through collagen affinity. *Sci. Transl. Med.* **11**, eaau3259 (2019).

Science Translational Medicine

Targeted antibody and cytokine cancer immunotherapies through collagen affinity

Jun Ishihara, Ako Ishihara, Koichi Sasaki, Steve Seung-Young Lee, John-Michael Williford, Mariko Yasui, Hiroyuki Abe, Lambert Potin, Peyman Hosseinchi, Kazuto Fukunaga, Michal M. Raczy, Laura T. Gray, Aslan Mansurov, Kiyomitsu Katsumata, Masashi Fukayama, Stephen J. Kron, Melody A. Swartz and Jeffrey A. Hubbell

Sci Transl Med **11**, eaau3259.
DOI: 10.1126/scitranslmed.aau3259

Conjugated bliss

Immunotherapies for cancer are becoming increasingly common due to their impressive ability to activate the patients' own immune system to fight tumors. However, systemic approaches to immune system activation are not risk free, and immunotherapies are often associated with corresponding immune side effects, which can be severe. To address this problem, Ishihara *et al*. conjugated immune checkpoint inhibitors and the cytokine interleukin-2 to the collagen-binding domain from a blood protein, allowing them to bind to tumor stroma and exert their effects locally. The researchers tested this approach in multiple mouse models, demonstrating improved efficacy and safety compared to the unconjugated molecules.